THE JOURNAL OF BIOLOGICAL CHEMISTRY
Vol. 277, No. 26, Issue of June 28, pp. 23807–23814, 2002

Printed in U.S.A.

Structure and Function of Human Erythrocyte Pyruvate Kinase

MOLECULAR BASIS OF NONSPHEROCYTIC HEMOLYTIC ANEMIA*

Received for publication, March 4, 2002, and in revised form, April 12, 2002
Published, JBC Papers in Press, April 17, 2002, DOI 10.1074/jbc.M202107200

Giovanna Valentini‡§¶, Laurent R. Chiarelli§, Riccardo Fortin‡, Manuela Dolzan‡, Alessandro Galizzi‡, Donald J. Abraham‖, Changqing Wang‖, Paola Bianchi, Alberto Zanella**, and Andrea Mattevi‡ ‡‡**

*From the ‡Dipartimento di Genetica e Microbiologia, Università di Pavia, via Abbiategrasso 207, 27100 Pavia, Italy, the §Dipartimento di Biochimica, Università di Pavia, via Taramelli 3b, 27100 Pavia, Italy, the ‖Department of Medicinal Chemistry, Virginia Commonwealth University, Richmond, Virginia 23219, and the **Divisione di Ematologia, IRCCS Ospedale Maggiore di Milano, via Francesco Sforza 35, 20122 Milano, Italy*

Deficiency of human erythrocyte isozyme (RPK) is, together with glucose-6-phosphate dehydrogenase deficiency, the most common cause of the nonspherocytic hemolytic anemia. To provide a molecular framework to the disease, we have solved the 2.7 Å resolution crystal structure of human RPK in complex with fructose 1,6-bisphosphate, the allosteric activator, and phosphoglycolate, a substrate analogue, and we have functionally and structurally characterized eight mutants (G332S, G364D, T384M, D390N, R479H, R486W, R504L, and R532W) found in RPK-deficient patients. The mutations target distinct regions of RPK structure, including domain interfaces and catalytic and allosteric sites. The mutations affect to a different extent thermostability, catalytic efficiency, and regulatory properties. These studies are the first to correlate the clinical symptoms with the molecular properties of the mutant enzymes. Mutations greatly impairing thermostability and/or activity are associated with severe anemia. Some mutant proteins exhibit moderate changes in the kinetic parameters, which are sufficient to cause mild to severe anemia, underlining the crucial role of RPK for erythrocyte metabolism. Prediction of the effects of mutations is difficult because there is no relation between the nature and location of the replaced amino acid and the type of molecular perturbation. Characterization of mutant proteins may serve as a valuable tool to assist with diagnosis and genetic counseling.

Pyruvate kinase (PK)[1] catalyzes the conversion of phosphoenolpyruvate (PEP) to pyruvate with the synthesis of ATP. The enzyme requires K^+ and Mg^{2+} (or Mn^{2+}) for activity (1–3). The PK-catalyzed reaction represents the last step of glycolysis with the reaction product, pyruvate, being involved in a number of energetic and biosynthetic pathways. PK is activated homotropically by PEP and heterotropically by monophosphorylated or bisphosphorylated sugars (2). In addition, Mg^{2+}, H^+, and other cations modulate enzymatic activity (4). The regulatory behavior of PK varies depending on the enzyme source. Four PK isozymes have been identified in mammals (5). The M1 (muscle) and M2 (fetal) proteins are products of the alternative splicing of the same mRNA. M2 PK is allosterically activated by fructose 1,6-bisphosphate (FBP) and PEP, whereas the M1 enzyme is exceptional in that it is the only known PK that displays hyperbolic kinetics. The other two mammalian PK isozymes, liver and erythrocyte, are coded by the same *PKLR* gene through the use of tissue-specific alternate promoters. Both erythrocyte and liver isozymes are activated by PEP and FBP (2).

The three-dimensional structures of several PKs from prokaryotic and eukaryotic organisms have been elucidated (6–10). They reveal a conserved architecture. PK is a 200-kDa tetramer with four identical subunits, each consisting of four domains (Fig. 1): the small N-terminal helical domain (absent in bacterial PKs); the A domain with $(\beta/\alpha)_8$ barrel topology; the B domain, which is inserted between strand $\beta3$ and helix $\alpha3$ of the A domain $(\beta/\alpha)_8$ barrel; and the C domain with an $\alpha+\beta$ topology. This multidomain architecture is instrumental to the regulation of PK activity. The enzyme activation is thought to involve a combination of domain and subunit rotations coupled to alterations in the active site geometry. In this mechanism, the residues located at the domain and subunit interfaces are crucial in that they function in the communication between the activator-binding site and the catalytic center (8–10).

Deficiency of human erythrocyte isozyme (RPK) is, together with glucose-6-phosphate dehydrogenase deficiency, the most common cause of nonspherocytic hemolytic anemia (11). RPK deficiency severely affects the erythrocyte metabolism, causing ATP depletion, which ultimately leads to hemolysis. Worldwide, more than 150 mutations in the gene coding RPK have been found in RPK-deficient patients (12). The disease is transmitted as a recessive trait, and the pathological symptoms occur only in homozygotes or compound heterozygotes. The clinical manifestations vary from mild to severe anemia, which can be life threatening and require continuous transfusion therapy. Here, we describe the first crystal structure of recombinant RPK and the biochemical characterization of eight mutants found in patients subjected to clinical follow-up. These

* This work was supported by grants from University of Pavia Progetto d'Ateneo "Nuove Tecnologie Molecolari e Cellulari," Ministero della Ricerca Scientifica e Tecnologica Progetto Genomica Funzionale, and Allos Therapeutics Inc. (Westminster, CO). The costs of publication of this article were defrayed in part by the payment of page charges. This article must therefore be hereby marked "*advertisement*" in accordance with 18 U.S.C. Section 1734 solely to indicate this fact.

The atomic coordinates and structure factors (code 1LIU, 1LIW, 1LIX, and 1LIY) have been deposited in the Protein Data Bank, Research Collaboratory for Structural Bioinformatics, Rutgers University, New Brunswick, NJ (http://www.rcsb.org/).

¶ To whom correspondence may be addressed. Fax: 39-0382-423108; E-mail: giovale@unipv.it.

‡‡ To whom correspondence may be addressed. Fax: 39-0382-528496; E-mail: mattevi@ipvgen.unipv.it.

[1] The abbreviations used are: PK, pyruvate kinase; RPK, human erythrocyte pyruvate kinase; PEP, phosphoenolpyruvate; FBP, fructose 1,6-bisphosphate; Mes, 4-morpholineethanesulfonic acid.

TABLE I
Data collection and refinement statistics

	Native	R479H	T384M	R486W
Space group	$P2_1$	$P2_1$	$P2_1$	$P2_1$
Unit cell axes *a*,*b*,*c* (Å)	74.4	74.0	76.3	73.7
	172.1	171.8	173.0	171.2
	85.5	85.1	85.8	85.0
β (°)	92.5	91.2	93.1	91.6
Completeness (%)[a]	95.9 (86.5)	92.6 (90.1)	93.7 (91.3)	89.0 (68.6)
Measured reflections	118,752	98,901	116,305	76,390
Unique reflections	55091	50701	52721	42512
Resolution (Å)	2.7	2.7	2.7	2.9
R_{sym} (%)[a,b]	7.6 (24.1)	9.5 (46.7)	7.9 (54.6)	10.3 (28.3)
Protein atoms	15,431	15,181	15,435	15,218
Solvent molecules	65	0	0	0
Ligand atoms	124	124	124	124
R-factor (%)[c]	23.0	24.2	24.6	24.3
R_{free} (%)[c]	27.9	29.0	30.0	30.9
Root mean square bond lengths (Å)	0.020	0.025	0.024	0.024
Root mean square bond angles (°)	2.0	2.4	2.8	2.9
Noncrystallographically symmetry-related, domains A and C (Å)[d]				
Subunit 1 to subunit 2	0.26	0.15	0.22	0.17
Subunit 1 to subunit 3	0.16	0.27	0.19	0.45
Subunit 1 to subunit 4	0.20	0.24	0.22	0.28
Noncrystallographically symmetry-related, domain B (Å)[d]				
Subunit 1 to subunit 2	0.37	0.32	0.31	0.26
Subunit 1 to subunit 3	0.33	0.40	0.32	0.33
Subunit 1 to subunit 4	0.31	0.37	0.43	0.38
Ramachandran plot (%)[e]				
Most favoured regions	89.9	86.6	86.7	83.2
Additionally allowed regions	9.5	12.4	12.6	15.6
Disallowed regions	0.5	0.9	0.7	1.2

[a] The values in parentheses are for reflections in the highest resolution shell.
[b] $R_{sym} = \Sigma|I_i - \langle I\rangle|/\Sigma I_i$, where I_i is the intensity of i^{th} observation and $\langle I\rangle$ is the mean intensity of the reflection.
[c] *R*-factor $= \Sigma|F_{obs} - F_{calc}|/\Sigma|F_{obs}|$, where F_{obs} and F_{calc} are the observed and calculated structure factor amplitudes, respectively.
[d] Root mean square deviation between Cα atoms of the noncrystallographically symmetry-related monomers present in the asymmetric unit. Tight noncrystallographically symmetry-related restraints were applied throughout the refinement.
[e] Analyzed with Procheck (38).

studies allow a correlation between the clinical symptoms and the molecular properties of the mutant enzymes.

EXPERIMENTAL PROCEDURES

Expression Vectors—The vectors used to express RPK and its mutant and truncated forms were derivatives of pTrcHisB (Invitrogen). RPK cDNA insert was obtained from pGG1 (13) after introduction of *Nco*I-*Nde*I sites around the ATG initiation codon. The mutagenic primer (14) used to introduce the two sites into pGG1 was 5′-CAAGGAGGCTGAAACCATGGCTAGCCAGGAGAACATATCATT. It altered the second and the third codon of the insert. The underlined letters indicate the mutated bases. The selection primer used to abolish the vector unique restriction site *Afl*III was 5′-CGCAGGAAAGACCTTGGGAGCAAAAGGCC. The pTrcHisB with RPK cDNA inserted in *Nco*I/*Eco*RI and designated pCW3 was mutagenized to restore the codons previously changed. The mutagenic primer was 5′-TAAGGAGGAATAAACCATGTCGATCCA GGAGAACATATCAT. The selection was performed by digesting the parental pCW3 with *Nco*I. The new plasmid, which contains the correct insert, was named pLC1. To obtain the desired RPK mutants, the pLC1 was subjected to site-directed mutagenesis (14). The same selection primer (5′-CCCCCCTGAATTCGAACCTTGGCTG) was used to abolish the unique *Hind*III site in all cases. The specific mutagenic primers were: 5′-CTGGAGGTGAGCGACAGCATCATGGTGGCA for G332S; 5′-CTGCAACTTGGCGGACAAGCCTGTTGTCTG for G364D; 5′-CAAGCCCCGGCCAATGAGGGCAGAGACAAG for T384M; 5′-AGGGCAGAGACAAGCAATGTCGCCAATGCTG for D390N; 5′-CTGACCACAACTGGCCACTCAGCCCAGCTTCTG for R479H; 5′-AGCCCAGCTTCTGTCTTGGTACCGACCTCGG for R486W; 5′-CTGCCCAGGCTGCCCTCCAGGTCCACTTAT for R504L; and 5′-ATGATGTAAGATCGCTGGGTGCAATTTGGCA for R532W. To obtain a truncated form of RPK lacking the first 49 residues, pCW3 was mutagenized by using the primer 5′-TAAGGAGGAATAAACC**ATG**GAGCTGGGCACTGCCTTCTTCC. This sequence corresponds to that of the plasmid upstream of the initiation triplet ATG and continues with that of the RPK insert starting from the GAG codon of Glu at position 50. The selection was performed by digesting pCW3 with *Nhe*I restriction enzyme. The plasmid with the insert encoding the truncated RPK (residues 50–574) was designated pLC3. All of the inserts were sequenced.

Protein Purification and Enzymatic Analysis—Escherichia coli DH5α transformed with the specific expression vectors were grown at 37 °C in Luria-Bertani medium containing 100 μg/ml ampicillin. When the culture optical density at 600 nm reached a value of 0.5, the expression was induced by addition of isopropyl-β-D-thiogalactopyranoside at a final concentration of 0.5 mM. The induction time was 12 h, whereas the induction temperature was 30 °C, with the exception of the mutants G332S, G364D, R504L, and R532W, for which the induction temperature was 21 °C. Wild-type and mutant enzymes were purified by the procedure of Wang *et al.* (13). Enzyme activities were measured at 37 °C by the assay (13) recommended by the International Committee for Standardization in Hematology. The kinetic parameters were determined with the Enzyme Kinetic Module™ 1.1 (SPSS Science Software Gmb). Thermal stability was measured by incubating the enzyme (100–200 μg/ml) at 53 °C in a solution consisting of 20 mM potassium phosphate, pH 6.5, 100 mM KCl, and 1 mM EDTA. The samples were removed at intervals and immediately assayed.

Crystallography—Recombinant wild-type RPK was crystallized using the vapor diffusion method at 22 °C. Well solutions consisted of 50 mM Mes/KOH, pH 6.4, 10 mM $MnSO_4$, and 10–14% w/v PEG8000. Hanging drops were formed by mixing equal volumes of 12 mg/ml protein in 50 mM KCl, 5 mM FBP, 5 mM phosphoglycolate, 20 mM potassium phosphate, pH 7.0, and well solutions. The crystals were difficult to reproduce. The recombinant enzyme undergoes partial proteolysis, and about 50% of the purified protein chains lack the first 47 amino acids (13). On this basis, we produced a mutant truncated en-

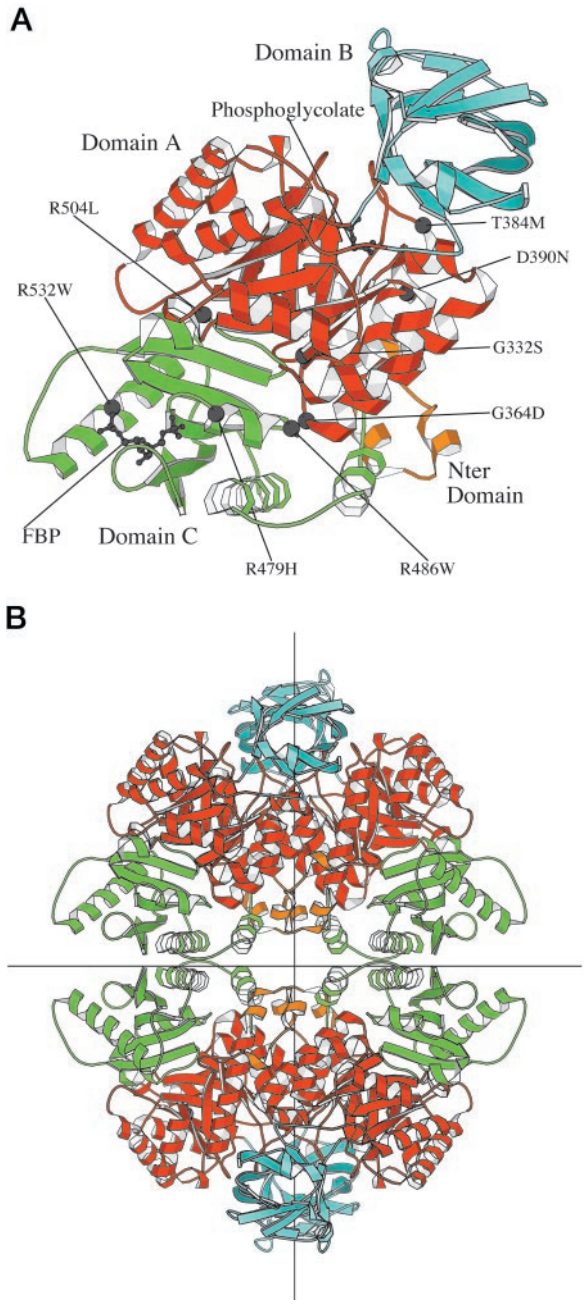

FIG. 1. **Three-dimensional crystal structure of RPK.** The N-terminal domain is *yellow*, the A domain is *red*, the B domain is cyan, and the C domain is *green*. *A*, the RPK subunit. The *gray spheres* indicate the Cα atoms of the residues subjected to mutagenesis. *B*, the RPK tetramer. In this orientation, a molecular 2-fold axis is perpendicular to the plane of the paper, whereas the other two molecular 2-fold axes are vertical and horizontal to the plane of the paper (indicated with *vertical* and *horizontal lines*, respectively).

zyme lacking the first 49 residues (see above). Employment of the truncated protein greatly improved the crystallization, which was carried out using the above-described protocol. Crystals were obtained for the T384M, R479H, and R486W truncated mutants by the same protocol used for the truncated wild-type RPK.

RPK crystals belong to space group $P2_1$ with one tetramer in the asymmetric unit. The diffraction data were measured at 100 K on beamline ID14-EH2 of the European Synchrotron Radiation Facility (Grenoble, France) using a MarCCD detector and beamline B7WB of DESY/EMBL (Hamburg, Germany) using a Mar Imaging Plate. Data processing and reduction were carried out using MOSFLM (15) and programs of the CCP4 suite (16). The data collection statistics are reported in Table I. The structure of the wild-type RPK was solved by molecular replacement using the program Molrep (16). The search model was the structure of rabbit muscle M1 PK in complex with pyruvate (Ref. 7; Protein Data Bank entry 1PKN). The Phases were improved by 4-fold averaging (17), producing an electron density of excellent quality. Model building was carried out with the program O (18). The model was refined using Refmac (19). All of the measured data (no σ cut-off) were employed, and 2.5% of unique reflections were used to monitor the progress of the refinement by R_{free} validation. The refined wild-type coordinates provided the starting model for the refinement of the mutants. The set of reflections for calculation of R_{free} was identical to that of the wild-type structure refinement. A summary of refinement statistics is presented in Table I. Analysis and inspection of the structures were carried out with the program O (18) and programs of the CCP4 package (16). The figures were generated with Molscript (20).

RESULTS

The Three-dimensional Structure of RPK—The crystallographic studies were performed using a truncated RPK in which the 49 N-terminal amino acids are absent. Use of the truncated protein resulted in considerable improvement in the reproducibility of the crystallization experiments. The truncated protein exhibits kinetic properties virtually identical to those of wild-type RPK. A more detailed analysis of this and other mutants targeting the N-terminal residues will be published elsewhere.

The truncated recombinant RPK was crystallized in complex with phosphoglycolate (a PEP analogue), FBP, Mn^{2+}, and K^+. The presence of the allosteric activators implies that the crystalline enzyme is in the active R state. The 2.7 Å resolution structure of RPK reveals the typical four-domain subunit architecture found in all PKs of known three-dimensional structure (Fig. 1*A*). The A (residues 85–159 and 263–431) and C domains (residues 432–574), together with the small N-terminal domain (residues 57–84), form the main body of the subunit. The B domain (residues 160–262) is loosely packed to the rest of the molecule and adopts slightly different orientations (about 4°) in the four crystallographically independent polypeptide chains. The four subunits of the RPK tetramer are assembled to form a D_2 symmetric oligomer. The intersubunit interactions define two large contact areas; the A/A′ interface involves the A domains of subunits related by the vertical 2-fold axis, as defined in Fig. 1*B*, whereas the C/C′ interface involves the C domains of subunits interacting along the horizontal axis.

The structure of the RPK subunit closely resembles that of rabbit muscle M1 PK, as expected from the 59% sequence identity between the two proteins. The similarity is highest with M1 PK in complex with pyruvate (7), with a root-mean-square difference of 1.2 Å for 512 Cα atom pairs. This M1 PK complex exhibits the same B domain orientation found in RPK. In other M1 structures, the B domain is either more open, as in the phospholactate complex (21), or more closed, as in the complex with ATP (22, 23).

The Allosteric Site and the Catalytic Center—RPK was cocrystallized with FBP, phosphoglycolate, and the K^+ and Mn^{2+} ions. All ligands are clearly visible in the electron density map. Phosphoglycolate, a potent PK inhibitor (9), is positioned in the PEP-binding site, which is located at the top of the A domain $(\beta/\alpha)_8$ barrel, facing a cleft between the A and B domains (Fig. 1*A*). It is at the heart of an intricate network of hydrogen bonds, which involve protein residues and the Mn^{2+} and K^+ cations (Fig. 2*A*). The phosphate group is bound to the K^+ atom and the side chain of Arg^{116}, whereas the carboxylate moiety is anchored through interactions with the Mn^{2+} ion, the side chain of Thr^{371}, and the main chain nitrogen atoms of Gly^{338} and Asp^{339}, which are located at the N terminus of a short helical segment belonging to loop 6 of the A domain $(\beta/\alpha)_8$ barrel. This binding geometry is identical to that observed in the yeast PK-phosphoglycolate complex (9) and closely resembles the

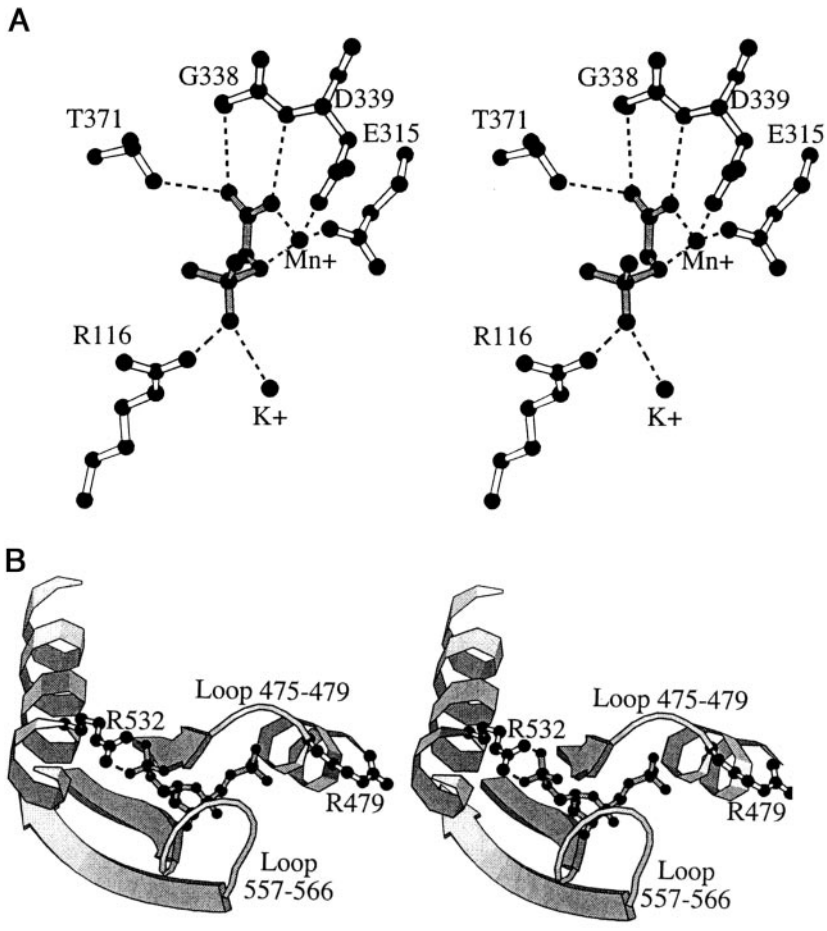

FIG. 2. **The allosteric and catalytic sites of RPK.** *A*, stereo view of the active site with bound phosphoglycolate (indicated by *gray bonds*), Mn^{2+}, and K^+. With respect to Fig. 1*A*, the model has been rotated by ~30° around an axis horizontal to the plane of the paper. *B*, stereo view of the allosteric site with bound FBP (*gray bonds*). The orientation is as in Fig. 1*A*.

TABLE II
Kinetic parameters of the wild-type and mutant RPKs
The results are the means ± S.E. for three determinations from four different protein preparations.

Enzyme	PEP[a]								ADP[b]		
	FBP(−)				1 mM FBP						
	k_{cat}	$S_{0.5}$	$k_{cat}/S_{0.5}$	n_H	k_{cat}	$S_{0.5}$	$k_{cat}/S_{0.5}$	n_H	k_{cat}	$S_{0.5}$	$k_{cat}/S_{0.5}$
	s^{-1}	mM	s^{-1}/mM		s^{-1}	mM	s^{-1}/mM		s^{-1}	mM	s^{-1}/mM
Wild type[c]	355 ± 12	1.10 ± 0.04	323	1.60 ± 0.16	355 ± 11	0.18 ± 0.020	1972	1.05 ± 0.07	355 ± 13	0.17 ± 0.01	2080
G332S	137 ± 6	3.79 ± 0.2	36	2.31 ± 0.12	152 ± 5	0.38 ± 0.04	389	1.08 ± 0.08	111 ± 7	0.49 ± 0.03	226
G364D	104 ± 7	0.93 ± 0.03	112	1.54 ± 0.03	118 ± 6	0.75 ± 0.02	153	1.39 ± 0.03	115 ± 6	0.16 ± 0.04	718
T384M	149 ± 10	1.24 ± 0.09	120	1.50 ± 0.03	172 ± 7	0.36 ± 0.07	383	1.00 ± 0.16	135 ± 9	0.15 ± 0.02	900
D390N	0.48 ± 0.04	1.40 ± 0.05	0.34	1.65 ± 0.01	0.55 ± 0.05	0.34 ± 0.009	1.6	1.15 ± 0.02	0.45 ± 12	0.25 ± 0.01	1.8
R479H	390 ± 8	1.10 ± 0.03	454	2.09 ± 0.02	386 ± 8	0.08 ± 0.003	4452	1.17 ± 0.06	381 ± 12	0.20 ± 0.02	1905
R486W	195 ± 4	1.69 ± 0.06	116	2.07 ± 0.11	203 ± 10	0.40 ± 0.07	492	1.32 ± 0.03	218 ± 13	0.24 ± 0.02	908
R504L	ND[c]	ND	ND	ND	ND	ND	ND	ND	ND	ND	ND
R532W	183 ± 5	0.63 ± 0.03	290	1.41 ± 0.11	187 ± 8	0.66 ± 0.06	275	1.48 ± 0.14	189 ± 12	0.20 ± 0.04	945

[a] Kinetic parameters for PEP were obtained at fixed 1.5 mM ADP by fitting data to the Hill plot.
[b] Kinetic parameters for ADP were obtained at fixed 5 mM PEP by fitting data to the Lineweaver-Burk plot.
[c] ND, not determined.

binding of pyruvate and phospholactate to rabbit M1 PK (for a discussion of the implications of this binding mode for catalysis see Refs. 7 and 21). These similarities are in keeping with the strict conservation among the PK sequences of all residues surrounding the substrate-binding site.

The FBP activator is hosted in the allosteric site in the C domain (Fig. 1*A*). The ligand is sandwiched between loops 475–479 and 557–566 (Fig. 2*B*) and extensively interacts with protein. The 6′-phosphate group is engaged in a salt bridge with Arg^{532}, whereas the 1′-phosphate is hydrogen-bonded to the side chains of Thr^{475} and Ser^{480} and the backbone nitrogen atoms of Thr^{476} and Thr^{477}. Moreover, the dipole of α-helix 480–486 points toward the 1′-phosphate, further compensating the ligand negative charge. This geometry in FBP-binding is identical to that found in yeast PK crystallized in the R state (9).

Rationale for the Mutagenesis Studies—A survey of the missense mutations associated with the nonspherocytic hemolytic anemia shows that most of them cluster in specific regions of the protein three-dimensional structure: the interface between the A and C domains, the A/A′ intersubunit interface, the hydrophobic core of the A domain, and the FBP-binding site (24). We generated eight RPK mutants (Fig. 1*A*), targeting residues belonging to each of these regions of the protein. Almost all selected mutations have been found in homozygote patients. The kinetic, allosteric, and thermostability parameters of mutant proteins were evaluated (Table II), and the crystal structures of three mutants (T384M, R479H and

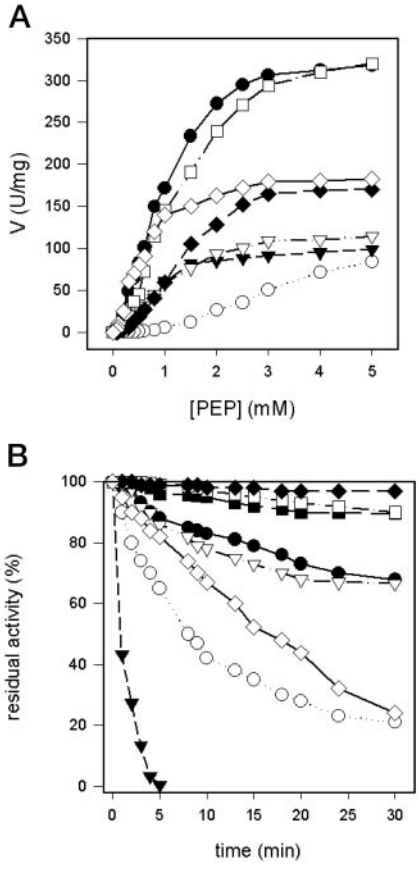

FIG. 3. **Characterization of RPK mutants.** ●, wild type; ○, G332S; ▼, G364D; ▽, T384M; ■, D390N; □, R479H; ◆, R486W; ◇, R532W. *A*, steady state kinetics of wild-type and mutant RPKs as a function of PEP. *B*, thermal stability of wild-type and mutant RPKs. The residual activity after incubation at 53 °C is expressed as a percentage of the initial activity.

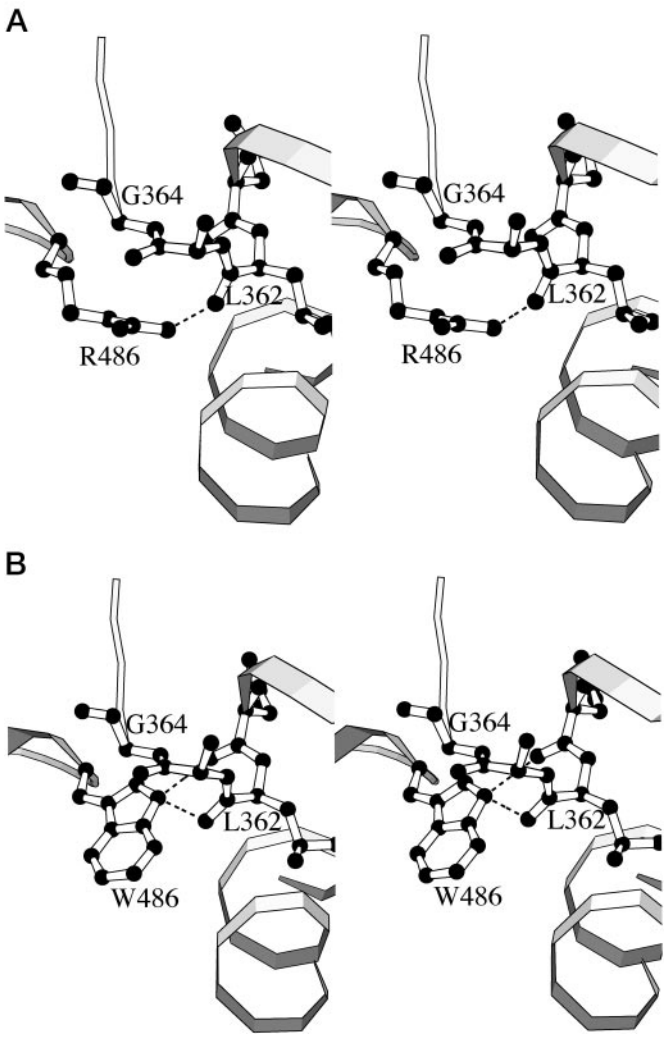

FIG. 4. **The A/C interface in the region surrounding Arg^{486}.** The orientation is as in Fig. 1*A*. *A*, stereo diagram of the wild-type structure. *B*, stereo diagram of the R486W mutant structure.

R486W) were solved. The mutations did not induce significant conformational changes in the overall protein conformation, and therefore we shall restrict the description of the mutant structures mainly to the sites affected by the mutations.

G332S Mutation in the A Domain Hydrophobic Core—Many RPK mutations are localized in the hydrophobic core of the A domain. An example is the G332S mutation (nucleotide G^{994} → A), which affects a residue that is strictly conserved among PK sequences. Gly^{332} is located on strand β6, being buried inside the domain core (Fig. 1*A*). The G332S protein exhibits a 9-fold decrease in the catalytic efficiency (5-fold for the FBP activated protein) and is considerably less thermostable than the wild-type enzyme (Table II and Fig. 3). These substantially altered molecular properties account for the clinical data. In homozygous form, the G332S mutation leads to severe anemia with the need of regular transfusions (25, 26).

Mutations at the A/C Interface: G364D, R486W, and R504L—The interface between the A and C domains is characterized by many polar interactions that often involve charged side chains. Many of these residues represent sites of pathological mutations, which cause RPK deficiency at variable levels of severity.

The mutation R504L (nucleotide G^{1511} → T) affects Arg^{504}, a C domain residue that is partly solvent-accessible and engaged in an interdomain salt bridge with Asp^{281} (Fig. 1*A*). The R504L mutation removes this interdomain interaction and introduces a hydrophobic Leu side chain in a solvent exposed site close to a negatively charged Asp. Such amino acid replacement is clearly unfavorable, providing a reason for the extreme instability of the protein, which prevented functional analysis (Table II). This feature explains the severe anemia found in RPK-deficient patients homozygous for this mutation (27).

The other two investigated mutants targeting the A/C interface affect Gly^{364} and Arg^{486}, which are part of a region of close association between the A and C domains (Figs. 1*A* and 4*A*). Arg^{486} is hydrogen-bonded to the carbonyl oxygen of Leu^{362} at the C terminus of the A domain helix α6, whereas the neighboring Gly^{364} allows a sharp turn of the polypeptide chain with a backbone conformation ($\phi = 85°, \psi = 98°$) that is unfavorable for a nonglycine residue. The G364D (nucleotide G^{1091} → A) mutation has a drastic effect on the enzyme stability, which is coupled to a 3-fold reduction of the catalytic efficiency (Fig. 3*B* and Table II). Given the tightly packed environment and the backbone conformation of Gly^{364}, it is conceivable that introduction of a charged Asp side chain at this site of the A/C interface can greatly perturb the domain assembly, thus being deleterious for stability. Fully consistent with these observations is the severe anemia found in patients homozygous for G364D (28). Together with R504L, the G364D mutant highlights the notion that the interdomain interactions at the A/C interface are critical for the stability of the protein.

R486W (nucleotide C^{1456} → T) is among the most frequent mutations found in RPK-deficient patients (11). Characterization of this mutant reveals that such a drastic amino acid replacement results in small effects on the molecular properties. The mutant three-dimensional structure shows that the

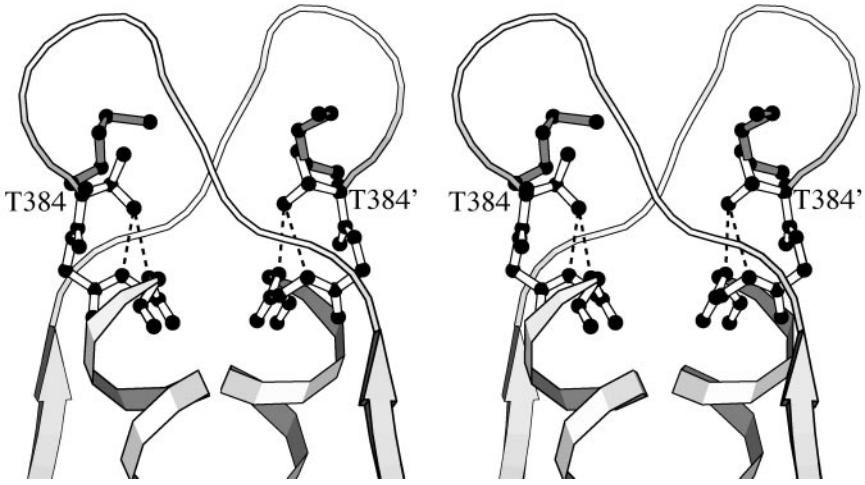

FIG. 5. **The A/A′ interface close to Thr^{384}.** The helices α7 of 2-fold related subunits are shown. The residues of the opposite subunits are denoted by the prime symbol. Attached to Thr^{384} is the Met side chain (*gray bonds*) of the crystal structure of the T384M mutant. The orientation is as in Fig. 1*A*.

Trp side chain is accommodated without any structural perturbation. With respect to the wild-type structure, no atomic movements larger than 0.25 Å can be detected, whereas the indole nitrogen atom is able to establish a hydrogen bond with the carbonyl oxygen atoms of Leu^{362} and Asp^{361}. Such structural conservation matches the limited changes in biochemical parameters. The thermostability is even higher than that of the wild-type protein (Fig. 3*B*), and the allosteric properties are essentially unmodified (Table II and Fig. 3*A*). The only significant perturbation is in the catalytic efficiency, which drops to 30% of the value measured for the wild-type RPK (Table II). These moderate variations in the molecular parameters correlate with the clinical symptoms because patients homozygous for the R486W mutation generally exhibit a mild anemia (25).

The perturbed kinetics of the R486W protein is puzzling because Arg^{486} is >20 Å away from the catalytic center (Fig. 1*A*), which is left unperturbed by the mutation as shown by the mutant crystal structure. The "long range" effect of the R486W mutation might reflect altered dynamic properties. It is known that the B domain adopts different conformations depending on ligand binding (21–23). The introduction of the Trp aromatic ring may restrict the overall ability of the enzyme to undergo the conformational changes occurring during catalysis, thereby perturbing the reaction kinetics.

The A/A′ Interface: T384M and D390N—Asp^{390} is a solvent-inaccessible residue located in the A/A′ interface, at the heart of a hydrogen bond network that involves Arg^{337} and Ser$^{389'}$ (the prime symbol denotes a residue of a different subunit). Based on the comparison between the structures of the *T* state *E. coli* PK and of the M1 isozyme, it was found that Asp^{390} is crucial for the allosteric transition by coupling changes in the quaternary structure with alterations in the active site geometry (8). A pathological mutation affecting this residue (D390N corresponding to nucleotide G^{1168} → A) has been detected in a heterozygote patient (25). The molecular analysis shows that the D390N amino acid replacement causes the almost complete inactivation of the protein, which, however, is not less thermostable than the wild-type RPK (Table I and Fig. 3*B*). These results are very similar to those obtained with the *E. coli* enzyme for which the same mutation was investigated (29). These observations support the idea that Asp^{390} has a key role in the allosteric regulation, suggesting that the D390N mutation may lock the protein in an inactive conformation, impairing the transition to the R state.

The mutation T384M (nucleotide C^{1151} → T) affects a residue, which, although not directly involved in intersubunit interactions, lays very close to the A/A′ molecular 2-fold axis (Fig. 5). Thr^{384} is located at the N terminus of helix α7 of the A domain $(\beta/\alpha)_8$ barrel. Its OG atom is hydrogen-bonded to the backbone nitrogen atoms of Ala^{386} and Glu^{387}, thus acting as helix-capping element. The three-dimensional structure of the T384M mutant reveals that the mutation does not cause atomic shifts larger than 0.3 Å (Fig. 5). The bulkier Met side chain is easily accommodated, the only change being the removal of the helix-capping hydrogen bonds. Also the kinetic characterization shows limited variations, the main difference between T384M and the wild-type protein being a 3-fold reduction of the catalytic efficiency (5-fold for the FBP activated form; Table II) that is mainly accounted for by a reduction in k_{cat}. Likewise, the mutation does not alter the thermostability parameters (Fig. 3).

Thr^{384} is not part of the binding sites for PEP and ADP, and the crystal structure of the T384M protein shows that the active site geometry is not affected by the mutation. Thus, the altered kinetics displayed by the T384M mutant is difficult to rationalize. Modified enzymatic parameters were observed also for the equivalent mutation in the rabbit kidney isozyme (30). Thr^{384} is close to the contact region between the A and B domains (Fig. 1*A*) and therefore the T384M mutation may disturb the "closure" of the B domain occurring upon ATP binding (22). An alteration of the equilibrium between the "open" and "closed" B domain conformations may affect the enzymatic activity. It is remarkable that homozygosity for the T384M mutation is associated with anemia with mild to severe symptoms (31, 32), implying that even moderate changes in the enzyme catalytic power can have pathological effects.

The Allosteric Site: R532W and R479H—The negative charges of FBP are compensated by the N terminus of helix 479–486 for the 1′-phosphate and Arg^{532} side chain for the 6′-phosphate (Fig. 2*B*). We have investigated two mutations that target both of the elements involved in FBP binding. The first of these mutations is R532W (nucleotide C^{1594} → T), which has been found in compound heterozygotes, in which the other allele had a mutation causing the truncation of the protein. The clinical symptoms in the patients carrying the mutation were severe (33). Molecular analysis of the R532W protein indicates a complete loss in the responsiveness to FBP, highlighting the essential Arg^{532} role in activator binding (Table II). These perturbed allosteric properties are associated with a decreased thermostability (Fig. 3*B*), possibly reflecting the energetically unfavorable exposure on the protein surface of the hydrophobic Trp residue.

The R479H mutation has been found in RPK-deficient patients affected by severe anemia (34, 35). The side chain of Arg^{479} is located in the neighborhood of FBP, although it does not directly interact with the activator (Fig. 2*B*). The crystal

structure of R479H is identical to that of the wild-type protein, with the His side chain being fully solvent-exposed. Similarly, the kinetic parameters (Table II) appear to be essentially unaffected by the mutation. These features are in contrast with the severe clinical symptoms (34, 35). An explanation for this riddle is given by the observation that the mutation affects nucleotide 1436, which is located on a splicing site at the 3′-end of exon 10. This fact, together with our biochemical analysis, suggests that, rather than the amino acid replacement, defects in mRNA splicing process are the actual cause of the RPK deficiency.

DISCUSSION

Implications for the Allosteric Regulation—PK is a typical allosteric enzyme of the K type. The allosteric signal is transmitted across the long distance (>20 Å) separating the FBP-binding site from the catalytic center. The exact mechanism of the allosteric transition is not known in detail because no PK has been so far crystallized in both the T and R states. The comparison between the structure of the T state *E. coli* PK and that of the rabbit M1 enzyme (8) suggested that the allosteric transition involves modifications in the relative orientations of the domains and subunits coupled to conformational changes in the PEP-binding site. The x-ray analysis of the T state *Leishmania mexicana* PK (10) and the R state yeast PK (9) led to a further refinement of this model, allowing a better discrimination between the structural differences that are consequences of the inherent divergence between eukaryotic and prokaryotic proteins and the conformational changes that are genuinely caused by the allosteric transition. The mechanism of PK regulation has also been the subject of many mutagenesis experiments (Refs. 23 and 36 and references therein). The general picture emerging from the mutant analysis is that the intersubunit interactions at the A/A′ and C/C′ interfaces and the interdomain interactions at the A/B interface are key to determining the allosteric responsiveness and to defining the distribution of the conformations between active and inactive states. Moreover, the mutagenesis analyses combined with the crystallographic data provide clear evidence for the idea that the T and R forms correspond to ensembles of conformations characterized by the rotational flexibility of the B domain (23).

Our study on human RPK is fully consistent with these features. The crystal structure shows that the B domain is flexible in RPK also, adopting different orientations in the crystallographically independent subunits. The key functional role of the A/A′ interface is highlighted by the D390N mutation, which targets a residue located in the core of the A/A′ interface, producing an enzyme that retains a stable tetrameric state but almost entirely lacks enzymatic activity. Conversely, none of the mutations targeting residues at the A/C interface alters the enzyme allosteric properties. Thus, in agreement with the recent mutagenesis data on the yeast PK (36), this domain interface appears to have little role in the transduction of the allosteric signal; rather it is important for the stability of the domain assembly within the enzyme subunit.

Molecular Basis of Nonspherocytic Hemolytic Anemia—Characterization of mutant proteins shows that amino acid substitutions can affect thermostability, catalytic efficiency, and response to the allosteric effector. Various regions of the RPK structure, including domain interfaces and functional sites, are affected by the pathological mutations (Fig. 1*A*). However, there appears to be no relation between the nature and location of the replaced amino acid and the type of molecular perturbation. For instance, both R504L and R486W mutations affect Arg residues involved in interdomain polar interactions at the A/C interface, but their effects are substantially different. The R504L protein is extremely unstable, whereas the R486W mutant is even slightly more thermoresistant than the wild type (Fig. 3*B*). These observations emphasize the difficulty of predicting the consequences of mutations simply from the location and the nature of the target residues. They also warn against predictions of the effects of mutations in human RPK based on the molecular analysis of other PK isozymes.

The clinical manifestations of a genetic disease reflect the interactions of a variety of physiological and environmental factors and do not solely depend on the molecular properties of the altered molecule. Given this caution, it is evident that there is a general correlation between the clinical manifestations and the biochemical parameters of the mutant proteins. Mutants exhibiting strongly perturbed kinetic and thermostability parameters (G332S, G364D, R504L, and R532W) are associated with severe RPK deficiency. Conversely, in the case of less abnormal molecular properties, the disease has milder manifestations. It is remarkable that pathological conditions are present in association with mutations such as T384M or R486W, which are simply characterized by a moderate reduction of the catalytic efficiency. The physiological concentrations of RPK substrates and effectors are in the micromolar range (37). Therefore, *in vivo* RPK operates in subsaturating conditions that may amplify the effects of the different catalytic efficiencies between the wild-type and mutant proteins (Fig. 3*A*).

In conclusion, our studies indicate that the functional parameters of RPK are so finely tuned that even moderate molecular alterations may significantly perturb cell metabolism. The correlation between molecular and clinical parameters in PK deficiency suggests that biochemical characterization of mutant proteins may serve as a valuable tool to understand and assist with diagnosis and genetic counseling.

Acknowledgments—We thank the staffs of the synchrotron beam lines of DESY/EMBL and ESRF for help during data collection.

REFERENCES

1. Kayne, F. J. (1973) *The Enzymes*, pp. 353–382, 3rd Ed., Academic Press Inc., New York
2. Fothergill-Gilmore, L. A., and Michels, P. A. (1992) *Prog. Mol. Biol. Biophys.* **59,** 105–227
3. Gupta, R. K., Oesterling, R. M., and Mildvan, A. S. (1976) *Biochemistry* **15,** 2881–2887
4. Mesecar, A. D., and Nowak, T. (1997) *Biochemistry* **36,** 6792–6802
5. Hall, E. R., and Cottam, G. L. (1978) *Int. J. Biochem.* **9,** 785–793
6. Allen, S. C., and Muirhead, H. (1996) *Acta Crystallogr. Sect. D Biol. Crystallogr.* **52**, 499–504
7. Larsen, T. M., Laughlin, L. T., Holden, H. M., Rayment, I., and Reed, G. H. (1994) *Biochemistry* **33,** 6301–6309
8. Mattevi, A., Valentini, G., Rizzi, M., Speranza, M. L., Bolognesi, M., and Coda A. (1995) *Structure* **3,** 729–741
9. Jurica, M. S., Mesecar, A., Heath, P. J., Shi, W., Nowak, T., and Stoddard, B. L. (1998) *Structure* **6,** 195–210
10. Rigden, D. J., Phillips, S. E. V., Michels, P. A. M., and Fothergill-Gilmore, L. A. (1999) *J. Mol. Biol.* **291,** 615–635
11. Zanella, A., and Bianchi, P. (2000) *Baillieres Best Pract. Res. Clin. Haematol.* **13,** 57–81
12. Bianchi, P., and Zanella, A. (2000) *Blood Cells Mol. Dis.* **26,** 47–53
13. Wang, C. Q., Chiarelli, L. R., Bianchi, P., Abraham, D. J., Galizzi, A., Mattevi, A., Zanella, A., and Valentini, G. (2001) *Blood* **98,** 3113–3120
14. Nickoloff, J. A., Deng, W. P., Miller, E. M., and Ray, F. A. (1996) *Methods Mol. Biol.* **58,** 455–468
15. Leslie A. G. (1999) *Acta Crystallogr. Sect. D Biol. Crystallogr.* **55**, 1696–1702
16. Collaborative Computational Project Number 4 (1994) *Acta Crystallogr. Sect. D Biol. Crystallogr.* **50**, 760–767
17. Cowtan, K. D., and Main, P. (1996) *Acta Crystallogr. Sect. D Biol. Crystallogr.* **52**, 43–48
18. Jones, T. A., Zou, J. Y., Cowan, S. W., and Kjeldgaard, M. (1991) *Acta Crystallogr. Sect. A* **47**, 110–119
19. Murshudov, G. N., Vagin, A. A., and Dodson, E. J. (1997) *Acta Crystallogr. Sect. D Biol. Crystallogr.* **53,** 240–255
20. Kraulis, P. J. (1991) *J. Appl. Crystallogr.* **24,** 946–950
21. Larsen, T. M., Benning, M. M., Wesenberg, G. E., Rayment I., and Reed, G. H. (1997) *Arch. Biochem. Biophys.* **345,** 199–206
22. Larsen, T. M., Benning, M. M., Rayment, I., and Reed, G. H. (1998) *Biochemistry* **37,** 6247–6255
23. Wooll, J. O., Friesen, R. H., White, M. A., Watowich, S. J., Fox, R. O., Lee, J. C.,

and Czerwinski, E. W. (2001) *J. Mol. Biol.* **312,** 525–540
24. Mattevi, A., Bolognesi, M., and Valentini, G. (1996) *FEBS Lett.* **389,** 15–19
25. Zanella, A., Bianchi, P., Baronciani, L., Zappa, M., Bredi, E., Vercellati, C., Alfinito, F., Pelissero, G., and Sirchia, G. (1997) *Blood* **89,** 3847–3852
26. Lenzner, C., Nurnberg, P., Thiele, B. J., Reis, A., Brabec, V., Sakalova, A., and Jacobasch, G. (1994) *Blood* **83,** 2817–2822
27. Demina, A., Varughese, K. I., Barbot, J., Forman, L., and Beutler, E. (1998) *Blood* **92,** 647–652
28. van Solinge, W. W., Kraaijenhagen, R. J., Rijksen, G., van Wijk, R., Stoffer, B. B., Gajhede, M., and Nielsen, F. C. (1997) *Blood* **90,** 4987–4995
29. Valentini, G., Chiarelli, L., Fortin, R., Speranza, M. L., Galizzi, A., and Mattevi, A. (2000) *J. Biol. Chem.* **275,** 18145–18152
30. Friesen, R. H., and Lee, J. C. (1998) *J. Biol. Chem.* **273,** 14772–14779
31. Kanno, H., Fujii, H., Hirono, A., and Miwa, S. (1991) *Proc. Natl. Acad. Sci. U. S. A.* **88,** 8218–8221
32. Neubauer, B., Lakomek, M., Winkler, H., Parke, M., Hofferbert, S., and Schröter, W. (1991) *Blood* **77,** 1871–1875
33. Lakomek, M., Huppke, P., Neubauer, B., Pekrun, A., Winkler, H., and Schroter, W. (1994) *Ann. Hematol.* **69,** 253–260
34. Kanno, H., Ballas, S. K., Miwa, S., Fujii, H., and Bowman, H. S. (1994) *Blood* **83,** 2311–2316
35. Kanno, H., Wei, D. C., Chan, L. C., Mizoguchi, H., Ando, M., Nakahata, T., Narisawa, K., Fujii, H., and Miwa, S. (1994) *Blood* **84,** 3505–3509
36. Fenton, A. W., and Blair, J. B. (2002) *Arch. Biochem. Biophys.* **397,** 28–39
37. Beutler, E. (1984) *Red Cell Metabolism: A Manual of Biochemical Methods*, Grune and Stratton, New York
38. Laskowski, R. A., MacArthur, M. W., Moss, D. S., and Thornton, J. M. (1993) *J. Appl. Crystallogr.* **26,** 283–291

Structure and Function of Human Erythrocyte Pyruvate Kinase: MOLECULAR BASIS OF NONSPHEROCYTIC HEMOLYTIC ANEMIA

Giovanna Valentini, Laurent R. Chiarelli, Riccardo Fortin, Manuela Dolzan, Alessandro Galizzi, Donald J. Abraham, Changqing Wang, Paola Bianchi, Alberto Zanella and Andrea Mattevi

J. Biol. Chem. 2002, 277:23807-23814.
doi: 10.1074/jbc.M202107200 originally published online April 17, 2002
